

Heavy quark suppression and anisotropic flow at intermediate momentum

Juhee Hong

*Department of Physics and Institute of Physics and Applied Physics,
Yonsei University, Seoul 03722, Korea*

(Dated: January 6, 2025)

Abstract

In an intermediate-momentum regime where mass effects are significant, heavy quark suppression and anisotropic flow are computed to investigate the transition between the collisional and radiative energy loss. Based on the collision kernel for diffusion, elastic scattering and semi-collinear gluon-bremsstrahlung can be consistently incorporated into a Boltzmann equation that involves the heavy quark diffusion coefficient. Using the running coupling constant and the diffusion coefficient constrained by lattice QCD data, the collisional and radiative energy-loss contributions to the R_{AA} and v_2 are studied in hydrodynamically expanding thermal media. The evolution of the observables, the bulk flow effect, and the dependence on mass and centrality are discussed in noncentral heavy-ion collisions.

I. INTRODUCTION

Heavy quark energy loss and jet quenching are important phenomena to understand the transport properties of quark-gluon plasmas(QGP) in relativistic heavy-ion collisions. Using various formalisms of energy loss, several transport models of heavy quarks have been developed, most of which, with some adjustment to model parameters, reasonably describe experimental data of heavy mesons [1–4]. Some of these models consider the collisional energy loss by elastic scattering only, while others also include the radiative one by gluon-bremsstrahlung. It is generally understood that heavy quark energy loss is dominated by elastic scattering and gluon emission at low and high momenta, respectively [1–4]. However, the intermediate-momentum region, where the heavy quark mass is nonnegligible, has large uncertainties regarding the significance of the radiative effect and the momentum-dependent transition between the relative dominance of the two mechanisms. Heavy quarks with finite mass and moderate momentum are particularly unique probes for studying the different energy-loss effects in QGP. To investigate the heavy quark energy loss in the intermediate-momentum region, a transport approach has recently been developed based on a Boltzmann equation with elastic scattering and semi-collinear gluon emission [5]. This approach enables distinct treatments of diffusion and radiation, while still describing both processes consistently through a single transport parameter, the heavy quark diffusion coefficient.

Heavy flavor interactions in strongly interacting QCD matter have mainly been studied with two experimental observables, the nuclear modification factor(R_{AA}) and the elliptic flow(v_2) which quantify medium modifications and momentum-space anisotropy, respectively. These observables are affected by numerous factors which include initial heavy quark production, expansion of background media, heavy quark interaction with QGP, hadronization, and hadronic rescattering. As a primary contribution to heavy flavor suppression, the heavy quark R_{AA} by energy loss has been investigated in Ref. [5]. This paper complements the previous work by applying the same formalism to noncentral heavy-ion collisions in order to compute both the suppression factor and the anisotropic flow of heavy quarks, which are induced by two types of energy loss. Although various approaches have been developed to estimate the degree of heavy quark energy loss and simultaneously describe R_{AA} and v_2 of heavy flavor, heavy quark modeling remains challenging [6, 7]. While the suppression factor is well-reproduced by transport models, the elliptic flow may be underestimated [1]. Compared to the R_{AA} , the v_2 is more complicated by initial fluctuations, bulk flow, and freezeout. Since there are multiple sources of azimuthal anisotropies through all stages of heavy-ion collisions, it is crucial to understand the energy-loss contribution to the heavy quark flow in the QGP phase.

The goal of this paper is to qualitatively examine how different types of energy loss contribute to the heavy flavor observables, R_{AA} and v_2 , in an intermediate-momentum regime. Sec. II begins with a brief review of heavy quark transport formulated in Ref. [5]. In Sec. III, the nuclear modification factor and the elliptic flow of heavy quarks are calculated in non-central heavy-ion collisions simulated with relativistic hydrodynamics. In expanding QGP, the evolution of two observables, the collisional and radiative energy-loss contributions, the bulk flow effect, and the dependence on impact parameter and mass are analyzed using the heavy quark diffusion coefficient which is constrained by lattice QCD data. Finally, Sec. IV provides a summary.

II. HEAVY QUARK DIFFUSION AND RADIATION

Heavy quarks undergo Brownian motion at low momentum, while medium-induced gluon emission dominates in the high-momentum limit. To study the transition from diffusion to radiation at intermediate momentum, a transport approach involving the heavy quark diffusion coefficient has been introduced in Ref. [5]. A brief review and the final form of the transport equation are provided in this section.

The heavy quark distribution function is determined by a Boltzmann equation with the collisional and radiative energy-loss terms,

$$\left(\frac{\partial}{\partial t} + \mathbf{v} \cdot \frac{\partial}{\partial \mathbf{x}} \right) f(t, \mathbf{x}, \mathbf{p}) = C_{\text{col}}[f] + C_{\text{rad}}[f]. \quad (1)$$

For soft momentum transfer, the collisional term can be approximated by a Fokker-Planck operator [8]

$$C_{\text{col}}[f] = \frac{\partial}{\partial p^i} [\eta(\mathbf{p}) p^i f(\mathbf{p})] + \frac{1}{2} \frac{\partial^2}{\partial p^i \partial p^j} [\kappa^{ij}(\mathbf{p}) f(\mathbf{p})], \quad (2)$$

where $\eta(\mathbf{p})$ is the drag coefficient and $\kappa^{ij}(\mathbf{p}) = \kappa_L(p) \hat{p}^i \hat{p}^j + \kappa_T(p) (\delta^{ij} - \hat{p}^i \hat{p}^j)$ is the momentum diffusion tensor. The drag coefficient is related to the longitudinal diffusion coefficient, $\eta(p) = \kappa_L(p)/(2TE_p) + \mathcal{O}(T/E_p)$, by the requirement of thermodynamic equilibrium in the large-time limit.

The formation time of gluon is given by the energy change in gluon-bremsstrahlung, $t_f = 2k(1-x)/(\mathbf{k}_T^2 + m^2 x^2 + m_g^2)$, where m is the heavy quark mass, $x = k/E_{\mathbf{p}+\mathbf{k}}$, $m_g^2 = m_D^2/2$ is the thermal mass of gluon, $E_{\mathbf{p}+\mathbf{k}}$ is heavy quark energy, $k \sim T$ and k_T are gluon energy and transverse momentum, respectively. To smoothly interpolate between low- and high-momentum regimes, a kinematic region where $gT \ll mx \ll T$ is considered. Since the formation time is shorter than the mean free path in this region, the gluon emission from a single scattering is used to compute the radiative term. In the semi-collinear limit, the gluon emission rate is [9–12]

$$\frac{d\Gamma(E_{\mathbf{p}}, k)}{dk} = \frac{g^2 C_F \kappa_T(p)}{\pi k} [1 + n_B(k)][1 - n_F(E_{\mathbf{p}-\mathbf{k}})] \times [(1-x)^2 + 1] \int \frac{d^2 \mathbf{p}_T}{(2\pi)^2} \frac{1}{(\mathbf{p}_T^2 + m^2 x^2 + m_g^2)^2}, \quad (3)$$

where $\Gamma(E_{\mathbf{p}}, k)$ is the rate for a heavy quark with momentum \mathbf{p} to emit a gluon with energy k . The rate has been found to be proportional to the diffusion coefficient, assuming that gluon has larger transverse momentum than soft momentum transfer. If $m^2 x^2$ is greater than \mathbf{p}_T^2 , gluon emission is suppressed at smaller angle than $\sim m/E_p$ [13]. In Eq. (1), the radiative energy loss is taken into account as follows:

$$C_{\text{rad}}[f] = \int dk \left[f(\mathbf{p} + \mathbf{k}) \frac{d\Gamma(E_{\mathbf{p}+\mathbf{k}}, k)}{dk} - f(\mathbf{p}) \frac{d\Gamma(E_{\mathbf{p}}, k)}{dk} \right] + \frac{1}{2} \nabla_{\mathbf{p}_T}^2 [\delta \kappa_T(p) f(\mathbf{p})], \quad (4)$$

where the first term is calculated in the eikonal approximation, $\mathbf{p} + \mathbf{k} \simeq (p+k)\hat{\mathbf{p}}$, the last term is the radiative correction to the approximation, and $k < 0$ corresponds to gluon absorption to satisfy detailed balance. The radiative correction to the transverse momentum

diffusion coefficient is given by

$$\delta\kappa_T(p) = \frac{g^2 C_F \kappa_T(p)}{2\pi} \int \frac{dk}{k} [(1-x)^2 + 1][1 + n_B(k)] \int \frac{d^2\mathbf{k}_T}{(2\pi)^2} \frac{k_T^2}{(\mathbf{k}_T^2 + m^2 x^2 + m_g^2)^2}, \quad (5)$$

which is $\mathcal{O}(g^2)$ suppressed more than the leading-order coefficient but logarithmically enhanced [14].

The heavy quark diffusion coefficient depending on momentum and temperature is important to determine the equilibration rate of heavy quarks in high-temperature QCD plasmas. The temperature dependence comes from running of the coupling constant: $\kappa_{L,T} \propto \alpha_s(E_p T) \alpha_s(m_D^2)$ [15]. In gluon-bremsstrahlung, the running coupling constant is determined at the scale, $Q^2 = (\mathbf{k}_T^2 + m^2 x^2 + m_g^2)/x$ [16]. As the temperature decreases, the coupling becomes stronger and nonperturbative effects start to enter. The momentum diffusion coefficient of a heavy quark grows as the momentum increases. By employing the leading-log momentum dependence [17], the static diffusion coefficient, $\kappa_{L,T}(p=0)$ which involves the nonperturbative effects, becomes the only transport parameter in Eq. (1). The momentum diffusion coefficient has been computed at next-to-leading order [18]. Since the convergence of the perturbative expansion is poor for a realistic value of the strong coupling, it is desirable to determine it using nonperturbative approaches such as lattice QCD computation [19–21] and phenomenological estimate [22, 23]. In this work, the momentum diffusion coefficient is constrained by lattice QCD data for the spatial diffusion coefficient, $D_s = 2T^2/\kappa_{L,T}(p=0)$. Through the lattice QCD data and the running coupling constant, nonperturbative effects can be absorbed at low momenta and temperatures near T_c .

III. NUCLEAR MODIFICATION FACTOR AND ELLIPTIC FLOW

The heavy quark Boltzmann equation of Sec. II has been solved for a Bjorken expansion to calculate the nuclear modification factor of heavy quarks [5]. This formulation provides a consistent description of the collisional and radiative energy loss, which exhibit different momentum dependence in an intermediate-momentum regime. The suppression factor is primarily determined by the collisional and radiative energy loss in the low and high momentum limit, respectively. The significance of the radiative effect at intermediate momentum is found to be influenced by the momentum and temperature dependence of the transport coefficients. Although heavy quark approximations may be only marginally satisfied for charm quarks, the transport equation has been applied to both charm and bottom quarks in order to demonstrate the impact of mass. In this section, the same equation is solved in noncentral collisions to compute both the suppression factor and the anisotropic flow which are induced by the heavy quark energy loss.

The anisotropic flow of heavy quarks is generated by asymmetric energy loss in noncentral heavy-ion collisions. A relativistic hydrodynamic simulation provides the time evolution of the spatial distributions of temperature and flow velocity fields which are anisotropic in the transverse plane. Initial conditions, especially the initial geometry and fluctuations of heavy-ion collisions, are a major source of significant uncertainties to determine QGP properties. Since this paper aims to qualitatively study how different mechanisms of energy loss influence the observables, a smooth initial distribution given by an optical Glauber model [24] is used. In a background medium generated by hydrodynamic simulations, Eq. (1) is solved with an initial condition where the momentum distribution is given by the differential cross section

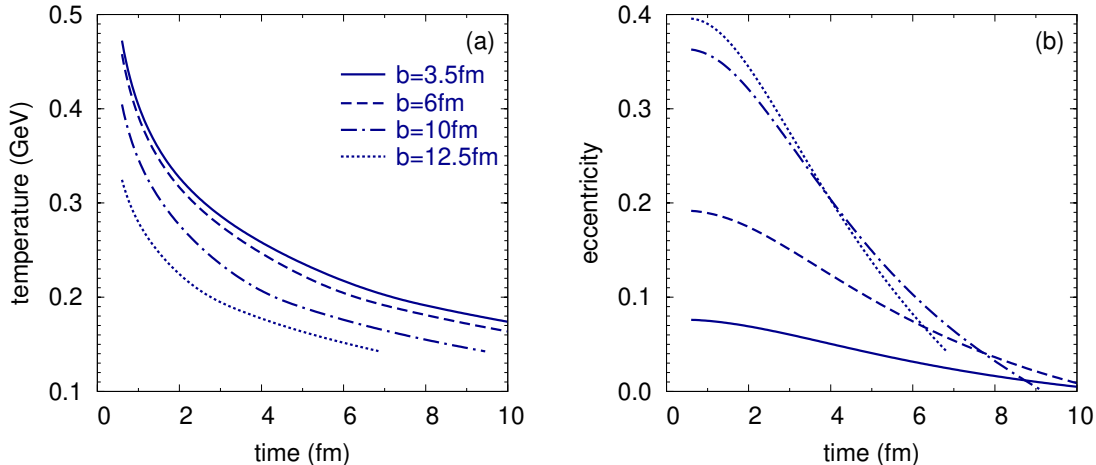


FIG. 1. Evolution of (a) the temperature at the center of thermal media and (b) the spatial eccentricity in noncentral PbPb collisions with $b = 3.5, 6, 10,$ and 12.5 fm.

of heavy meson measured in pp collisions [25, 26] and the spatial distribution is given by the same Glauber model,

$$f_{\mathbf{x}}(\mathbf{x}_T) = \int dz dz' \rho(\mathbf{x}_T + \frac{\mathbf{b}}{2}, z) \rho(\mathbf{x}_T - \frac{\mathbf{b}}{2}, z'), \quad (6)$$

where \hat{z} is the beam axis and the impact parameter \mathbf{b} is along the \hat{x} direction. A Woods-Saxon form of density, $\rho(r) \propto 1/[1 + \exp((r - R_0)/a)]$, is used with $R_0 = 6.62$ fm, $a = 0.546$ fm for PbPb collisions.

A. Expanding QGP

In noncentral collisions with nonzero impact parameter, the elliptic deformation of thermal media can be quantified with the spatial eccentricity,

$$\epsilon_2 = \frac{\langle y^2 - x^2 \rangle}{\langle y^2 + x^2 \rangle}, \quad (7)$$

where the brackets denote averaging with the energy density as a weighting factor. Because of the geometric deformation in the overlap region of two nuclei, the average velocity is larger in the \hat{x} direction than \hat{y} . In the hydrodynamic picture, this spatial anisotropy is transferred to the momentum space through the pressure gradients [27]. While the collective flow of light particles is effectively described by hydrodynamics, heavy quarks interacting with a background medium acquire various sources of azimuthal anisotropies through all stages of heavy-ion collisions. This work focuses on the energy-loss contribution to the heavy flavor flow in the QGP phase.

Figure 1 shows typical evolution of the QGP temperature at the center ($x = 0, y = 0$) and the spatial eccentricity in noncentral PbPb collisions. They are simulated with (3+1)-dimensional hydrodynamics code MUSIC [28–30] using the following hydrodynamic parameters¹: the initial time, $t_0 = 0.6$ fm, the maximum energy density, $e_0 = 100$ GeV/fm³, the

¹ These parameters have been chosen to produce the maximum temperature similar to that in Ref. [31]. Larger e_0 should generally be used to create higher-temperature plasmas at greater collision energies.

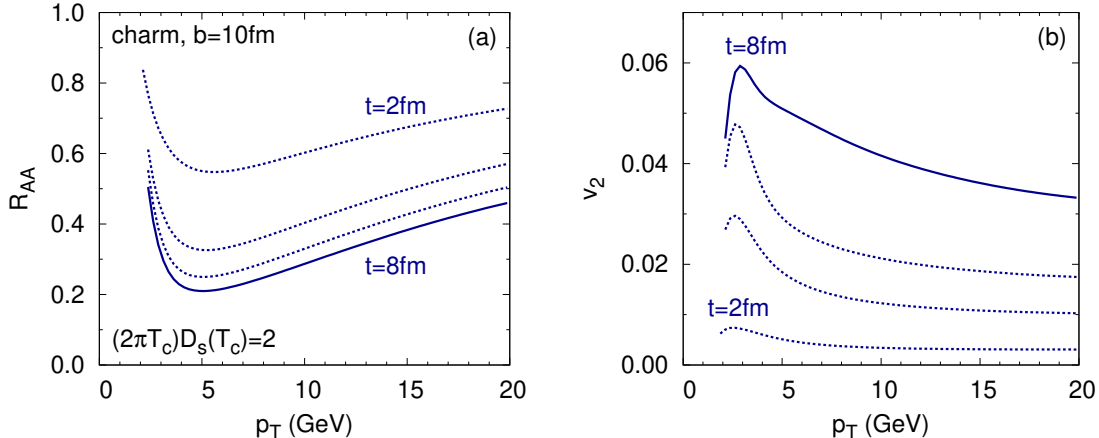


FIG. 2. (a) The nuclear modification factor and (b) the elliptic flow of charm quarks at $t = 2, 4, 6,$ and 8 fm.

ratio of shear viscosity to entropy density, $\eta/s = 0.08$, and the equation of state from lattice QCD data [32]. In more central collisions with smaller impact parameters, the maximum temperature is higher and the initial spatial eccentricity is lower. While the temperature and the spatial eccentricity decrease with time, the momentum anisotropy is expected to increase. Since heavy quarks are not fully thermalized within the lifetime of QGP, they do not follow the bulk flow of a background medium. In response to an initial spatial deformation, heavy quarks acquire the momentum anisotropy through coupling to the collective motion of the medium. In the following subsections, the profiles in the transverse plane, with the temperature at the center and the spatial eccentricity shown in Fig. 1, are used to calculate the heavy quark flow and the suppression factor at midrapidity.

B. Evolution of R_{AA} and v_2

At each position and time, heavy quarks experience the collisional and radiative energy loss which are controlled by the diffusion coefficient depending on temperature and flow velocity. Once the temperature drops below $T_c \sim 157$ MeV [33], heavy quarks are treated as free-streaming. After solving Eq. (1), the transverse momentum spectrum of heavy quarks is obtained by $\frac{dN}{d^2\mathbf{p}_T} = \int d^2\mathbf{x}_T f(t, \mathbf{x}_T, \mathbf{p}_T)$. The suppression factor is determined by the ratio of the quenched transverse momentum spectrum to the unquenched spectrum without the energy-loss effect. The collective flow is quantified in terms of Fourier components of the azimuthal angle distribution:

$$\frac{dN}{d^2\mathbf{p}_T} = \frac{1}{2\pi} \frac{dN}{p_T dp_T} \left[1 + 2 \sum_n v_n(p_T) \cos n\phi \right]. \quad (8)$$

Ignoring higher-order harmonics, $R_{AA}^{\text{in,out}}(p_T) = R_{AA}(p_T)[1 \pm 2v_2(p_T)]$, where the superscripts in $R_{AA}^{\text{in,out}}$ denote in-plane ($\phi = 0$) and out-of-plane ($\phi = \pi/2$). The azimuthally averaged suppression factor is $R_{AA}(p_T) = [R_{AA}^{\text{in}}(p_T) + R_{AA}^{\text{out}}(p_T)]/2$, and the elliptic flow is estimated

as [34, 35]

$$v_2(p_T) = \frac{1}{2} \frac{R_{AA}^{\text{in}}(p_T) - R_{AA}^{\text{out}}(p_T)}{R_{AA}^{\text{in}}(p_T) + R_{AA}^{\text{out}}(p_T)}. \quad (9)$$

The nuclear modification factor of heavy quarks indicates the energy-loss effects in QGP, while the elliptic flow reflects how heavy quarks are distributed in the transverse plane and how they are correlated with the flowing thermal media. The anisotropic flow arises due to the asymmetric energy loss: heavy quarks out-of-plane cross longer paths of hot media so they experience more energy loss than those in-plane. Since R_{AA}^{out} is smaller than R_{AA}^{in} , heavy quarks obtain positive elliptic flow.

Figure 2 shows the evolution of the suppression factor and the anisotropic flow of charm quarks (with the charm-quark mass $m = 1.5$ GeV) for $b = 10$ fm. The R_{AA} factor decreases with time and saturate at $t \approx 8$ fm when the plasma reaches the critical point. Meanwhile, v_2 continuously increases. The elliptic flow is affected by the different path-length as well as the anisotropic temperature and collective flow. In contrast to R_{AA} which decreases mostly in the high-temperature plasmas at early times, v_2 buildup dominates at late times when the bulk flow is large and the heavy quark coupling with the medium is strong. Similar behavior in the time evolution has been observed previously [36]. Although the interaction rate is high and the flow transfer is efficient in the early stages, it takes time for the flow to accumulate. Due to the development at later times, a significant contribution to v_2 is also expected at the hadronic phase. Furthermore, v_2 may be more sensitive than R_{AA} to variations of T_c and the uncertainties in the freezeout prescription.

C. Collisional and radiative energy loss with D_s

The heavy quark formalism of Sec. II consistently describes both diffusion and radiation processes through D_s in an intermediate-momentum regime. The medium modification by gluon emission has been found to be distinguishable, exhibiting different momentum dependence compared to elastic scattering [5]. In this subsection, the radiative effect on both R_{AA} and v_2 is investigated in hydrodynamically expanding media.

Figure 3 (a) shows the nuclear modification factor of charm quarks, determined by each energy-loss mechanism. The solid lines are the suppression factors calculated with the running coupling constant and the momentum-dependent diffusion coefficients, and the dashed lines are those with constant coupling and diffusion coefficient. Similar patterns of the medium modifications to Ref. [5] have been observed with an adjustment to D_s . The R_{AA} by the radiative energy loss starts at $R_{AA} = 1$ for low momentum and consistently decreases as the momentum increases², while the R_{AA} by the collisional energy loss decreases at low momentum but increases at intermediate momentum. As a result, the dominant energy loss shifts from collisional to radiative as the heavy quark momentum increases. The transition momentum is dependent on the transport coefficients and their dependence on momentum and temperature: since the radiative effect is more significant with $\alpha_s = 0.3$ for gluon emission in the current numerical analysis, this transition occurs at higher momentum when $\kappa_{L,T}$ increases with momentum and α_s decreases with temperature, compared to when they are constant.

² No gluon emission is expected when $p_T \lesssim m$. In the high-momentum limit, the gluon emission rate must be calculated in multiple soft scatterings, and the radiative energy loss will be reduced due to the LPM effect [37, 38].

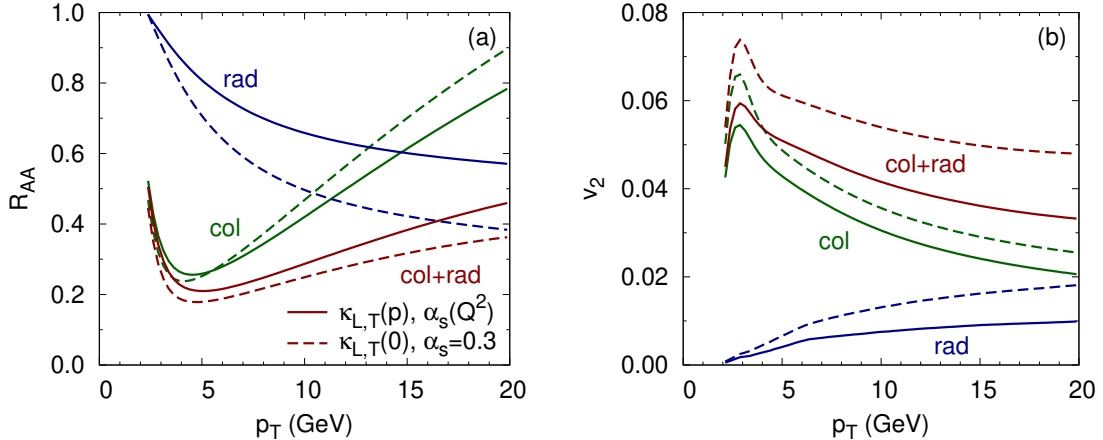


FIG. 3. The collisional and radiative energy-loss contributions to (a) the nuclear modification factor and (b) the elliptic flow of charm quarks with $(2\pi T_c)D_s(T_c) = 2$ in PbPb collisions with $b = 10$ fm. The solid lines show the calculated results using the momentum-dependent $\kappa_{L,T}$ and running coupling α_s , and the dashed lines show those with the constant diffusion coefficient and $\alpha_s = 0.3$ for gluon emission.

The collisional and radiative energy-loss contributions to the anisotropic flow are shown in Fig. 3 (b). As discussed in the previous paragraph, the momentum dependence of two energy-loss mechanisms is qualitatively distinct. While the collisional energy loss is dominant at low p_T , the radiative effect increases with the heavy quark momentum. The v_2 of charm quarks peaks at ~ 3 GeV and decreases as the momentum increases: the radiative effect slows this decline. As in R_{AA} , the radiative energy loss with $\alpha_s = 0.3$ is larger than that with running coupling.

In this paper, the heavy flavor observables have been calculated with the momentum-dependent diffusion coefficients and the running coupling constant, unless explicitly mentioned otherwise.

D. Bulk flow effect

To compute the R_{AA} and v_2 , the transverse momentum spectrum of heavy quarks is determined by heavy quark interactions in hydrodynamically expanding QGP. The interactions with a thermal medium can be characterized by the heavy quark diffusion coefficient, and its momentum and temperature dependence (through the running coupling constant) have been discussed in Sec. III C. This subsection now focuses on the influence of an expanding medium.

Given (t, \mathbf{x}_T) , a hydrodynamic simulation provides the temperature and the flow velocity field which are anisotropic in the transverse plane. For an expanding medium, the local rest frame of the medium is different from the lab frame where $\Delta \mathbf{x}_T = \frac{\mathbf{p}_T}{E_p} \Delta t$ is satisfied. $\Delta t'$ and $\Delta \mathbf{x}'_T$ in the local rest frame are given by $\Delta t' = \frac{E'_p}{E_p} \Delta t$ and $\Delta \mathbf{x}'_T = \frac{\mathbf{p}'_T}{E_p} \Delta t$ (where the energies and momenta in two frames are related through the Lorentz transformation with the flow velocity), respectively [39–41]. Using the flow velocity, the heavy quark distribution is updated according to Eq. (1) in the local rest frame of the medium. The heavy quark

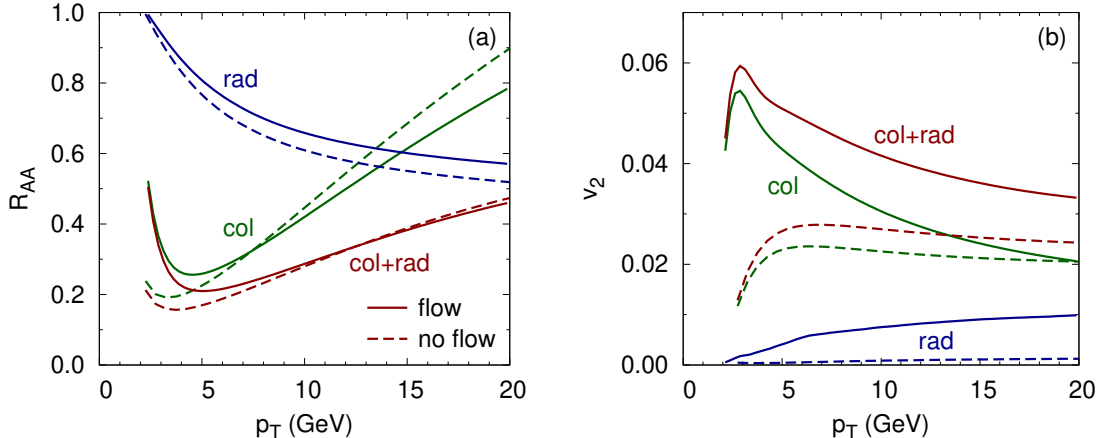


FIG. 4. The bulk flow effect on (a) the suppression factor and (b) the anisotropic flow of charm quarks with $(2\pi T_c)D_s(T_c) = 2$ for $b = 10$ fm. The solid and dashed lines correspond to the results with and without the radial flow of an expanding medium, respectively.

diffusion coefficient which determines the energy loss depends on both the temperature and flow velocity of an expanding medium. Thus, the transverse momentum spectrum in an expanding medium is influenced by bulk flow as well as by the asymmetric energy loss along different paths in an elliptically deformed medium. To investigate the contribution of bulk flow to the heavy flavor observables, the R_{AA} and v_2 have been computed in the anisotropic temperature distribution of plasmas with and without the radial flow.

In Fig. 4, the solid and dashed lines represent the results with and without the bulk flow, respectively. The bulk flow seems to shift the suppression factor to higher p_T , and the R_{AA} becomes larger at low momentum. Since this effect is greater for in-plane than out-of-plane, the elliptic flow is also enhanced. The contribution of bulk flow is particularly significant to v_2 at low p_T where v_2 exhibits a characteristic peak near ~ 3 GeV for charm quarks. On the other hand, the high- p_T region is mainly determined by the asymmetric energy loss with the path-length difference due to the initial geometric deformation. The bulk flow effect on R_{AA} and v_2 has been investigated in Refs. [40, 42]: although the exact effect depends on the energy loss model, the shift of R_{AA} to higher p_T and the enhancement of v_2 at low p_T are qualitatively consistent with the previous observations.

E. Impact parameter and mass effect

For noncentral heavy-ion collisions in Fig. 1, this subsection discusses the heavy flavor observables, focusing on the dependence on impact parameter and mass. The dependence on impact parameter is roughly related to the centrality dependence [43]. In realistic collisions with event-by-event fluctuations, heavy-ion collisions with the same impact parameter can produce different initial eccentricities. However, this work uses a smooth initial condition given by an optical Glauber model, so the eccentricity and the impact parameter are monotonically correlated.

Figure 5 shows the suppression factor and the elliptic flow of charm quarks with $(2\pi T_c)D_s(T_c) = 2 - 3$ which are closely aligned with lattice QCD data [19–21]. The

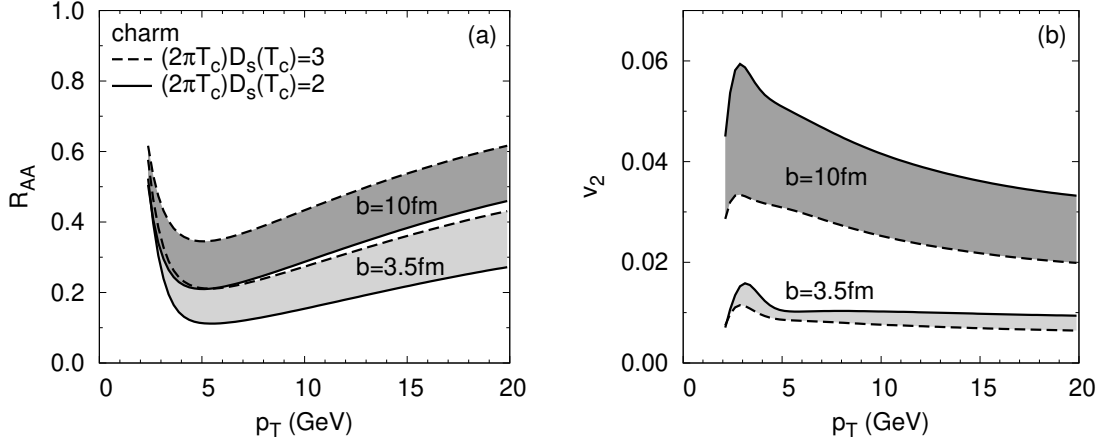


FIG. 5. (a) The nuclear modification factor and (b) the elliptic flow of charm quarks with $(2\pi T_c)D_s(T_c) = 2 - 3$ in noncentral PbPb collisions with $b = 3.5, 10$ fm.

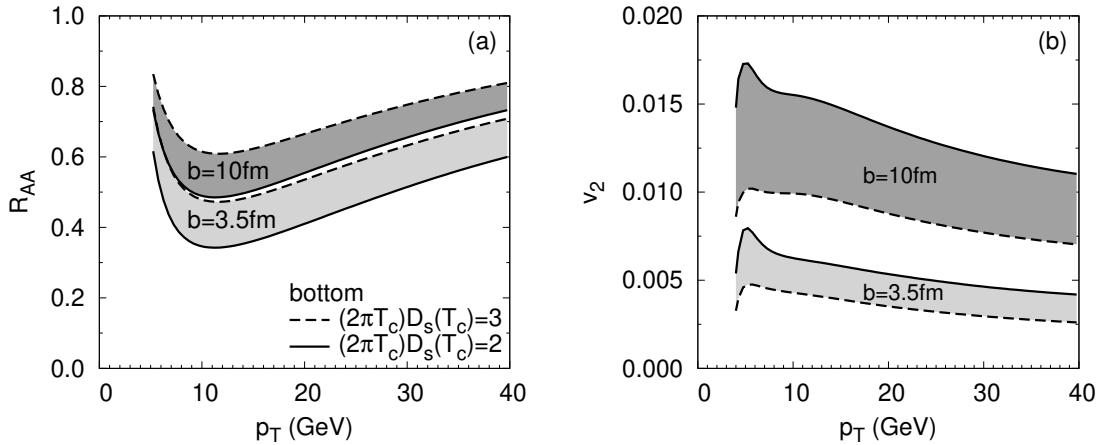


FIG. 6. Same as Fig. 5 but for bottom quarks.

heavy quark transport parameter determines the degree of heavy quark energy loss: as D_s decreases, both the collisional and radiative energy loss increase. Thus, the nuclear modification factor becomes smaller, and the anisotropic flow increases for smaller D_s . For fixed D_s , the R_{AA} factor at $b = 3.5$ fm is smaller than at $b = 10$ fm because the energy loss in more central collisions is larger due to bigger size and higher temperature of plasmas. On the other hand, the elliptic flow at $b = 3.5$ fm is smaller than at $b = 10$ fm because the initial eccentricity is greater in more peripheral collisions.

The suppression factor and the anisotropic flow of bottom quarks are shown in Fig. 6. Using the bottom-quark mass, $m = 4.5$ GeV, and the same value for the diffusion coefficient, both the collisional and radiative energy loss of bottom quarks are smaller than those of charm quarks. Thus, bottom quarks are less suppressed and the momentum-space anisotropy is also weaker.

The $R_{AA}(p_T)$ and $v_2(p_T)$ of D , B mesons have been measured [22, 26, 44, 45], and bottom energy loss has been investigated through nonprompt D meson [46, 47] in PbPb collisions

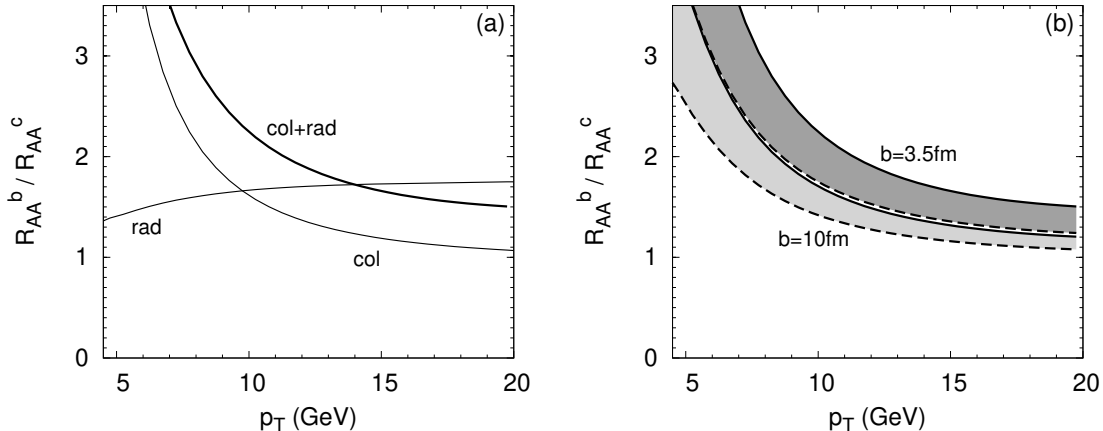


FIG. 7. (a) The ratio of bottom to charm quark R_{AA} at $b = 3.5$ fm, determined by the different mechanisms of energy loss. (b) The ratios by the total energy loss at $b = 3.5, 10$ fm, with $(2\pi T_c)D_s(T_c) = 2$ (solid lines) and $(2\pi T_c)D_s(T_c) = 3$ (dashed lines).

at LHC. Despite numerous efforts to develop the transport models of heavy quarks, it remains demanding to describe two quantities simultaneously. Since the observables of the heavy mesons are also influenced by factors other than the heavy quark interaction in QGP, the results of Figs. 5 and 6 should not be directly compared with the experimental data. However, their behavior, depending on the centrality(impact parameter), mass, and momentum, is similar to the measurements. In particular, the calculated suppression factors appear to be comparable with the data, whereas the prediction of the anisotropic flow is underestimated. Compared to R_{AA} , v_2 is more sensitive to the details of the transport models, such as the heavy quark transport coefficients and the centrality-dependent medium evolution with hydrodynamic flow [48]. For example, given the same $R_{AA}(p_T)$, 2 – 3 times larger $v_2(p_T)$ can be predicted by different temperature dependence of the heavy quark drag coefficient [7]. Since the elliptic flow is primarily developed at the later stages of the QGP evolution, hadronization [49, 50] and the freezeout prescription are also essential to determine v_2 ³. Especially, coalescence considerably enhances the elliptic flow at low momentum [52, 53], transferring the collective flow from medium to heavy mesons. For a more quantitative analysis, realistic initial conditions, including fluctuations, should also be applied and the hydrodynamic parameters must be adjusted to describe the soft sector prior to heavy quark study [54, 55]. This will be addressed in future work.

A comparison between the R_{AA} factors of bottom and charm quarks is motivated by the measurements of the nonprompt to prompt D^0 -meson R_{AA} ratio [47]. Fig. 7 (a) shows the ratio of bottom to charm quark R_{AA} , which implies the mass-dependent energy loss. Because the energy loss of charm quarks are larger than that of bottom quarks, R_{AA}^b/R_{AA}^c is bigger than unity. In particular, the radiative effect becomes significant to determine the ratio as the momentum increases. The ratio given by the total energy loss is notably enhanced at low p_T , then decreases as p_T increases, approaching unity: an analogous result has been obtained in Ref. [56] excluding coalescence which is effective at low momentum. The average ratio of the nonprompt to prompt D^0 -meson R_{AA} is 1.70 ± 0.18 [47] which is

³ The elliptic flow might arise from heavy quarks decoupling at different stages of QGP [51].

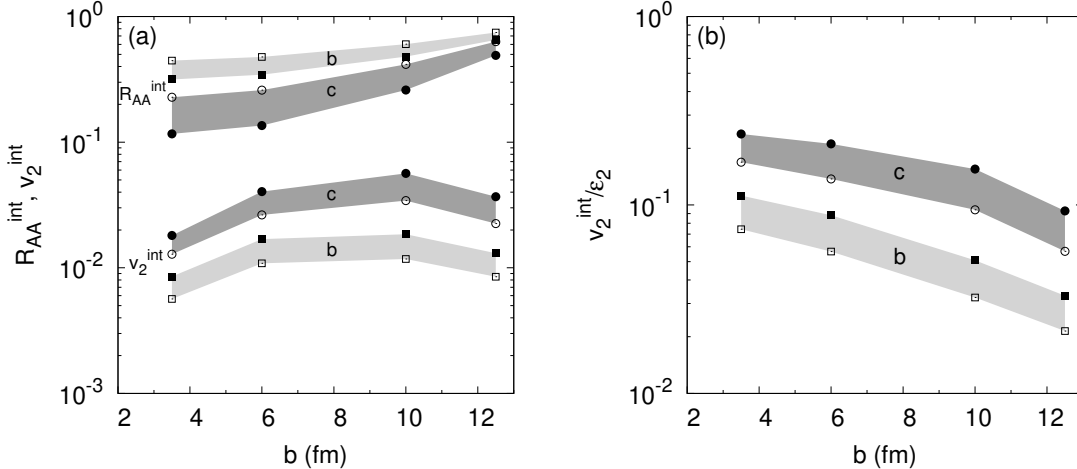


FIG. 8. (a) The p_T -integrated R_{AA} and v_2 as functions of impact parameter. (b) The ratio of the p_T -integrated v_2 to the initial spatial eccentricity. The constant transport coefficients $(2\pi T)D_s(T) = 2$ (closed symbols), $(2\pi T)D_s(T) = 3$ (open symbols), and $\alpha_s = 0.3$ for gluon emission have been used.

comparable with the calculated R_{AA}^b/R_{AA}^c near $p_T \sim 20$ GeV (where the coalescence effect is negligible). In more peripheral collisions where the energy-loss difference between bottom and charm quarks is smaller, the ratio is reduced, as shown in Fig. 7 (b).

To closely investigate the correlation between R_{AA} and v_2 , and their dependence on D_s , mass, and impact parameter, the p_T -integrated elliptic flow is defined as follows:

$$v_2^{\text{int}}(b) = \frac{\int dp_T p_T v_2(p_T, b) \frac{1}{2\pi} \frac{dN}{p_T dp_T}}{\int dp_T p_T \frac{1}{2\pi} \frac{dN}{p_T dp_T}}, \quad (10)$$

where $4 < p_T < 20$ GeV, and similarly for $R_{AA}^{\text{int}}(b)$. Fig. 8 (a) shows the integrated R_{AA} and v_2 of charm and bottom quarks in four noncentral heavy-ion collisions. While R_{AA} and v_2 as functions of p_T depend on the specifics of the heavy quark interaction in expanding QGP, the p_T -integrated observables generally exhibit the following centrality-dependent behavior. The integrated R_{AA} increases with b as the energy loss is larger in more central collisions where QGP have bigger size and higher temperature (longer lifetime)⁴. On the other hand, the integrated v_2 grows with b up to $b \sim 10$ fm after which it decreases for more peripheral collisions. The elliptic flow of heavy quarks is influenced by two competing effects, the geometric deformation and energy loss [57]. As b increases, the geometric asymmetry becomes bigger while the energy loss effect becomes smaller. A similar centrality-dependent behavior has been shown in the p_T -dependent R_{AA} and v_2 of Ref. [57]. The D_s and mass dependence of the integrated R_{AA} and v_2 remain the same as discussed in the p_T -dependent observables.

The heavy quark interaction and the coupling to QGP are weaker in more peripheral collisions [42]. As the impact parameter increases, the efficiency of transferring an initial geometric deformation to the momentum-space anisotropy decreases. Fig. 8 (b) shows the ratio of the p_T -integrated v_2 to the initial spatial eccentricity. The v_2^i/ϵ_2 decreases as the impact parameter increases, and the ratio of bottom quarks is smaller than that of charm quarks.

⁴ See Fig. 1 (a). The initial overlap area of two nuclei at $b = 3.5$ fm is about 3 – 4 times as large as that at $b = 12.5$ fm.

IV. SUMMARY

To demonstrate the transition between the collisional and radiative energy loss, heavy quark suppression and anisotropic flow have been computed in an intermediate-momentum regime where the finite mass is nonnegligible. For diffusion and semi-collinear gluon-bremsstrahlung, the qualitative features of the two energy-loss mechanisms have been consistently investigated by using the heavy quark diffusion coefficient of lattice QCD data. The p_T -dependent R_{AA} and v_2 induced by the radiative energy loss are found to be distinguishable from those caused by the collisional energy loss. By slowing the increase of $R_{AA}(p_T)$ and the decreases of $v_2(p_T)$, the radiative effect makes the observables more independent of p_T in the intermediate-momentum region, compared to those entirely determined by the collisional effect.

The numerical analysis indicates that a significant part of the heavy meson suppression results from the energy loss of heavy quarks particularly in the early stages of QGP. In contrast, the elliptic flow is influenced by the interplay between the energy loss and the spatial eccentricity in noncentral heavy-ion collisions, with its growth being considerable at late times. The contribution of bulk flow is found to be important at low momentum, especially to v_2 . The energy-loss difference between charm and bottom, as well as the centrality-dependence of the observables, has been discussed.

Reference [5] has presented a transport formulation for heavy quark diffusion and radiation with a single transport parameter, and this work conducts the numerical analysis in hydrodynamically expanding media. They provide a useful approach to exploring the intermediate-momentum regime, where the dominant energy loss shifts from elastic scattering to gluon-bremsstrahlung. The distinct medium modifications help clarify the relative importance of the two mechanisms and their influence on the heavy flavor observables. The observables are primarily determined by the collisional energy loss at low momentum, while the influence of the radiative effect increases as the heavy quark momentum grows. Although several transport models of heavy quarks are available to describe experimental data, this approach may offer a new perspective on the emergence of the radiative effect in the heavy quark energy loss.

ACKNOWLEDGMENTS

I would like to thank Sangyong Jeon and Su Houng Lee for useful comments. This work was supported by the National Research Foundation of Korea(NRF) grant funded by the Korea government(MSIT) (RS-2024-00342514) and Basic Science Research Program funded by the Ministry of Education (No. 2021R1I1A1A01054927).

-
- [1] A. Andronic, F. Arleo, R. Arnaldi, A. Beraudo, E. Bruna, D. Caffarri, Z. Conesa del Valle, J. G. Contreras, T. Dahms and A. Dainese, *et al.* Eur. Phys. J. C **76**, no.3, 107 (2016) [arXiv:1506.03981 [nucl-ex]].
 - [2] X. Dong, Y. J. Lee and R. Rapp, Ann. Rev. Nucl. Part. Sci. **69**, 417-445 (2019) [arXiv:1903.07709 [nucl-ex]].

- [3] L. Apolinário, Y. J. Lee and M. Winn, *Prog. Part. Nucl. Phys.* **127**, 103990 (2022) [arXiv:2203.16352 [hep-ph]].
- [4] M. He, H. van Hees and R. Rapp, *Prog. Part. Nucl. Phys.* **130**, 104020 (2023) [arXiv:2204.09299 [hep-ph]].
- [5] J. Hong, *Phys. Rev. C* **109**, no.2, 024913 (2024) [arXiv:2308.14530 [hep-ph]].
- [6] M. Djordjevic, *Phys. Rev. Lett.* **112**, no.4, 042302 (2014) [arXiv:1307.4702 [nucl-th]].
- [7] S. K. Das, F. Scardina, S. Plumari and V. Greco, *Phys. Lett. B* **747**, 260-264 (2015) [arXiv:1502.03757 [nucl-th]].
- [8] B. Svetitsky, *Phys. Rev. D* **37**, 2484-2491 (1988).
- [9] P. B. Arnold, G. D. Moore and L. G. Yaffe, *JHEP* **06**, 030 (2002) [arXiv:hep-ph/0204343 [hep-ph]].
- [10] J. Ghiglieri, J. Hong, A. Kurkela, E. Lu, G. D. Moore and D. Teaney, *JHEP* **05**, 010 (2013) [arXiv:1302.5970 [hep-ph]].
- [11] J. Ghiglieri and D. Teaney, *Int. J. Mod. Phys. E* **24**, no.11, 1530013 (2015) [arXiv:1502.03730 [hep-ph]].
- [12] J. Ghiglieri, G. D. Moore and D. Teaney, *JHEP* **03**, 095 (2016) [arXiv:1509.07773 [hep-ph]].
- [13] Y. L. Dokshitzer and D. E. Kharzeev, *Phys. Lett. B* **519**, 199-206 (2001) [arXiv:hep-ph/0106202 [hep-ph]].
- [14] T. Liou, A. H. Mueller and B. Wu, *Nucl. Phys. A* **916**, 102-125 (2013) [arXiv:1304.7677 [hep-ph]].
- [15] S. Peigne and A. Peshier, *Phys. Rev. D* **77**, 114017 (2008) [arXiv:0802.4364 [hep-ph]].
- [16] M. Djordjevic and M. Djordjevic, *Phys. Lett. B* **734**, 286-289 (2014) [arXiv:1307.4098 [hep-ph]].
- [17] G. D. Moore and D. Teaney, *Phys. Rev. C* **71**, 064904 (2005) [arXiv:hep-ph/0412346 [hep-ph]].
- [18] S. Caron-Huot and G. D. Moore, *Phys. Rev. Lett.* **100**, 052301 (2008) [arXiv:0708.4232 [hep-ph]].
- [19] D. Banerjee, S. Datta, R. Gavai and P. Majumdar, *Phys. Rev. D* **85**, 014510 (2012) [arXiv:1109.5738 [hep-lat]].
- [20] A. Francis, O. Kaczmarek, M. Laine, T. Neuhaus and H. Ohno, *Phys. Rev. D* **92**, no.11, 116003 (2015) [arXiv:1508.04543 [hep-lat]].
- [21] L. Altenkort *et al.* [HotQCD], *Phys. Rev. Lett.* **132**, no.5, 051902 (2024) [arXiv:2311.01525 [hep-lat]].
- [22] S. Acharya *et al.* [ALICE], *JHEP* **01**, 174 (2022) [arXiv:2110.09420 [nucl-ex]].
- [23] Y. Xu, J. E. Bernhard, S. A. Bass, M. Nahrgang and S. Cao, *Phys. Rev. C* **97**, no.1, 014907 (2018) [arXiv:1710.00807 [nucl-th]].
- [24] M. L. Miller, K. Reygers, S. J. Sanders and P. Steinberg, *Ann. Rev. Nucl. Part. Sci.* **57**, 205-243 (2007) [arXiv:nucl-ex/0701025 [nucl-ex]].
- [25] S. Acharya *et al.* [ALICE], *Eur. Phys. J. C* **79**, no.5, 388 (2019) [arXiv:1901.07979 [nucl-ex]].
- [26] A. M. Sirunyan *et al.* [CMS], *Phys. Rev. Lett.* **119**, no.15, 152301 (2017) [arXiv:1705.04727 [hep-ex]].
- [27] J. Y. Ollitrault, *Phys. Rev. D* **46**, 229-245 (1992).
- [28] B. Schenke, S. Jeon and C. Gale, *Phys. Rev. C* **82**, 014903 (2010) [arXiv:1004.1408 [hep-ph]].
- [29] B. Schenke, S. Jeon and C. Gale, *Phys. Rev. Lett.* **106**, 042301 (2011) [arXiv:1009.3244 [hep-ph]].
- [30] J. F. Paquet, C. Shen, G. S. Denicol, M. Luzum, B. Schenke, S. Jeon and C. Gale, *Phys. Rev. C* **93**, no.4, 044906 (2016) [arXiv:1509.06738 [hep-ph]].

- [31] W. M. Alberico, A. Beraudo, A. De Pace, A. Molinari, M. Monteno, M. Nardi, F. Prino and M. Sitta, *Eur. Phys. J. C* **73**, 2481 (2013) [arXiv:1305.7421 [hep-ph]].
- [32] P. Huovinen and P. Petreczky, *Nucl. Phys. A* **837**, 26-53 (2010) [arXiv:0912.2541 [hep-ph]].
- [33] A. Bazavov *et al.* [HotQCD], *Phys. Lett. B* **795**, 15-21 (2019) [arXiv:1812.08235 [hep-lat]].
- [34] J. Xu, A. Buzzatti and M. Gyulassy, *JHEP* **08**, 063 (2014) [arXiv:1402.2956 [hep-ph]].
- [35] B. B. Abelev *et al.* [ALICE], *Phys. Rev. C* **90**, no.3, 034904 (2014) [arXiv:1405.2001 [nucl-ex]].
- [36] R. Rapp and H. van Hees, [arXiv:0803.0901 [hep-ph]].
- [37] L. D. Landau and I. Pomeranchuk, *Dokl. Akad. Nauk Ser. Fiz.* **92**, 535-536 (1953).
- [38] A. B. Migdal, *Phys. Rev.* **103**, 1811-1820 (1956).
- [39] R. Baier, A. H. Mueller and D. Schiff, *Phys. Lett. B* **649**, 147-151 (2007) [arXiv:nucl-th/0612068 [nucl-th]].
- [40] S. Cao, T. Luo, G. Y. Qin and X. N. Wang, *Phys. Rev. C* **94**, no.1, 014909 (2016) [arXiv:1605.06447 [nucl-th]].
- [41] W. Ke, [arXiv:2001.02766 [nucl-th]].
- [42] M. Nahrgang, J. Aichelin, S. Bass, P. B. Gossiaux and K. Werner, *Phys. Rev. C* **91**, no.1, 014904 (2015) [arXiv:1410.5396 [hep-ph]].
- [43] W. Broniowski and W. Florkowski, *Phys. Rev. C* **65**, 024905 (2002) [arXiv:nucl-th/0110020 [nucl-th]].
- [44] A. Hayrapetyan *et al.* [CMS], [arXiv:2409.07258 [nucl-ex]].
- [45] G. Aad *et al.* [ATLAS], *Phys. Lett. B* **807**, 135595 (2020) [arXiv:2003.03565 [nucl-ex]].
- [46] S. Acharya *et al.* [ALICE], *Eur. Phys. J. C* **83**, no.12, 1123 (2023) [arXiv:2307.14084 [nucl-ex]].
- [47] S. Acharya *et al.* [ALICE], *JHEP* **12**, 126 (2022) [arXiv:2202.00815 [nucl-ex]].
- [48] A. Beraudo, A. De Pace, M. Monteno, M. Nardi and F. Prino, *Eur. Phys. J. C* **79**, no.6, 494 (2019) [arXiv:1812.08337 [physics.data-an]].
- [49] R. Rapp, P. B. Gossiaux, A. Andronic, R. Averbeck, S. Masciocchi, A. Beraudo, E. Bratkovskaya, P. Braun-Munzinger, S. Cao and A. Dainese, *et al.* *Nucl. Phys. A* **979**, 21-86 (2018) [arXiv:1803.03824 [nucl-th]].
- [50] J. Zhao, J. Aichelin, P. B. Gossiaux, A. Beraudo, S. Cao, W. Fan, M. He, V. Minissale, T. Song and I. Vitev, *et al.* *Phys. Rev. C* **109**, no.5, 054912 (2024) [arXiv:2311.10621 [hep-ph]].
- [51] A. Beraudo, A. De Pace, M. Monteno, M. Nardi and F. Prino, *JHEP* **02**, 043 (2018) [arXiv:1712.00588 [hep-ph]].
- [52] M. He, R. J. Fries and R. Rapp, *Phys. Rev. C* **86**, 014903 (2012) [arXiv:1106.6006 [nucl-th]].
- [53] A. Beraudo, A. De Pace, M. Monteno, M. Nardi and F. Prino, *Eur. Phys. J. C* **82**, no.7, 607 (2022) [arXiv:2202.08732 [hep-ph]].
- [54] M. Kurian, M. Singh, V. Chandra, S. Jeon and C. Gale, *Phys. Rev. C* **102**, no.4, 044907 (2020) [arXiv:2007.07705 [hep-ph]].
- [55] M. Singh, M. Kurian, S. Jeon and C. Gale, *Phys. Rev. C* **108**, no.5, 054901 (2023) [arXiv:2306.09514 [nucl-th]].
- [56] S. Li, W. Xiong and R. Wan, *Eur. Phys. J. C* **80**, no.12, 1113 (2020) [arXiv:2012.02489 [hep-ph]].
- [57] W. J. Xing, S. Q. Li, S. Cao and G. Y. Qin, *Phys. Rev. C* **110**, no.2, 024903 (2024) [arXiv:2404.12601 [hep-ph]].